DOI:
10.1016/j.neuroimage.2013.07.045

Document Version
Publisher's PDF, also known as Version of record

NeuroImage 83 (2013) 901–911

Contents lists available at SciVerse ScienceDirect

NeuroImage

journal homepage: www.elsevier.com/locate/ynimg

Normalization of similarity-based individual brain networks from gray matter MRI and its association with neurodevelopment in infants with intrauterine growth restriction

Dafnis Batalle [a,*], Emma Muñoz-Moreno [a], Francesc Figueras [a,b,c], Nuria Bargallo [d,e], Elisenda Eixarch [a,b,c], Eduard Gratacos [a,b,c]

[a] Fetal and Perinatal Medicine Research Group, Institut d'Investigacions Biomediques August Pi i Sunyer (IDIBAPS), Barcelona, Spain
[b] Maternal-Fetal Medicine Department, ICGON, Hospital Clínic, Universitat de Barcelona, Barcelona, Spain
[c] Centro de Investigación Biomédica en Red de Enfermedades Raras (CIBERER), Barcelona, Spain
[d] Centre de Diagnòstic per la Imatge Clínic (CDIC), Hospital Clínic, Barcelona, Spain
[e] Clinical Imaging Research, Institut d'Investigacions Biomediques August Pi i Sunyer (IDIBAPS), Barcelona, Spain

ARTICLE INFO

Article history:
Accepted 16 July 2013
Available online 22 July 2013

Keywords:
Brain morphology
Children
Connectome
Graph theory
Neurodevelopment
Bayley Scale for Infant and Toddler Development

ABSTRACT

Obtaining individual biomarkers for the prediction of altered neurological outcome is a challenge of modern medicine and neuroscience. Connectomics based on magnetic resonance imaging (MRI) stands as a good candidate to exhaustively extract information from MRI by integrating the information obtained in a few network features that can be used as individual biomarkers of neurological outcome. However, this approach typically requires the use of diffusion and/or functional MRI to extract individual brain networks, which require high acquisition times and present an extreme sensitivity to motion artifacts, critical problems when scanning fetuses and infants. Extraction of individual networks based on morphological similarity from gray matter is a new approach that benefits from the power of graph theory analysis to describe gray matter morphology as a large-scale morphological network from a typical clinical anatomic acquisition such as T1-weighted MRI. In the present paper we propose a methodology to normalize these large-scale morphological networks to a brain network with standardized size based on a parcellation scheme. The proposed methodology was applied to reconstruct individual brain networks of 63 one-year-old infants, 41 infants with intrauterine growth restriction (IUGR) and 22 controls, showing altered network features in the IUGR group, and their association with neurodevelopmental outcome at two years of age by means of ordinal regression analysis of the network features obtained with Bayley Scale for Infant and Toddler Development, third edition. Although it must be more widely assessed, this methodology stands as a good candidate for the development of biomarkers for altered neurodevelopment in the pediatric population.

Introduction

In recent years, the potential of brain magnetic resonance imaging (MRI) to detect brain alterations that can be related to a different range of neurological pathologies has been clearly demonstrated (Bassett and Bullmore, 2009; Eliez and Reiss, 2000; Horsfield and Jones, 2002). An additional area of importance in the application of the different modalities of MRI has been the development of connectomics (Hagmann, 2005) to extract features of the macroscopic circuitry of the connections of the brain, which has been called "the connectome" (Sporns et al., 2005). In particular, the use of graph theory analyses on brain networks has been a useful tool to characterize brain function by use of a few comprehensible parameters. For example, different sets of data, including functional MRI and diffusion MRI, have been used to extract macroscopic brain networks and analyze network features in healthy adults, adolescents and infants (Gong et al., 2009; Hagmann et al., 2008, 2010; Iturria-Medina et al., 2008; Yap et al., 2011) and to report altered group connectivity parameters in a wide range of neurological, neurobehavioral and neurodegenerative diseases by means of connectomic analysis (Alexander-Bloch et al., 2010; Liu et al., 2008; Lo et al., 2010; Shu et al., 2009, 2011; Wang et al., 2009; Wu et al., 2009). Importantly, connectomics and graph theory features are potential tools to develop biomarkers to predict neurological outcomes in adult (He et al., 2009; Li et al., 2009; Wee et al., 2010; Wen et al., 2011) and perinatal diseases (Batalle et al., 2012; Tymofiyeva et al., 2012).

However, although the use of diffusion and functional MRI are being more frequently applied, these techniques are still not very common in

Abbreviations: AAL, automated anatomical labeling; BSID-III, Bayley scale for infant development, third edition; CSF, cerebrospinal fluid; FDR, False Discovery Rate; GA, gestational age; GM, gray matter; IUGR, intrauterine growth restriction; MRI, magnetic resonance imaging; WM, white matter.

* Corresponding author at: Fetal and Perinatal Medicine Research Group, Hospital Clínic, IDIBAPS, Sabino de Arana 1, Helios III, 08028 Barcelona, Spain. Fax: +34 93 227 9336.
E-mail addresses: dbatalle@clinic.ub.es (D. Batalle), emunozm@clinic.ub.es (E. Muñoz-Moreno), figueras@clinic.ub.es (F. Figueras), bargallo@clinic.ub.es (N. Bargallo), eixarch@clinic.ub.es (E. Eixarch), gratacos@clinic.ub.es (E. Gratacos).

1053-8119/$ – see front matter © 2013 Elsevier Inc. All rights reserved.
http://dx.doi.org/10.1016/j.neuroimage.2013.07.045

clinical practice compared with conventional anatomical T1 acquisitions. In addition, the requirement of higher acquisition times and the extreme sensitivity to motion artifacts of diffusion and functional MRI is critical when scanning subjects where control of movements cannot be assured, such as fetuses or infants. Based on the concept that correlations of gray matter (GM) features such as volume or cortical thickness across groups of individuals are associated with brain connectivity (He et al., 2007), anatomical T1 acquisitions have been used to obtain group connectomes that allow for a better understanding of brain circuitry in health and disease (Bassett et al., 2008; Fan et al., 2011; He et al., 2008). However, in order to develop individual biomarkers, it is indispensable to extract individual brain networks, which typically requires diffusion and/or functional MRI. Recently, a number of published reports have suggested approaches to extract individual brain networks based on the analysis of the similarities of GM features (Raj et al., 2010; Tijms et al., 2012, 2013; Zhou et al., 2011). These methodologies can benefit from the power of brain network analysis to predict individual neurological outcome, albeit using conventional T1 acquisitions. To what extent these networks resemble anatomical brain networks is an issue that still remains to be elucidated. Regardless of whether the brain networks reconstructed resemble actual anatomical networks or just serve to analyze cortical pattern similarities, this approach has the potential to become a powerful tool in clinical practice if it allows obtaining features associated with the neurological outcome of different diseases.

In the present paper we extend the work of Tijms et al. (2012) that allows the generation of individual morphology similarity-based structural brain networks from MRI. Specifically, we propose a methodology that allows normalization of the large-scale networks obtained to a common framework, so that each subject network has the same network size, which has some clear advantages in order to perform comparative analyses (van Wijk et al., 2010). We prove the feasibility and utility of this approach by applying it to a specific disease. Namely, we used late-onset intrauterine growth restriction (IUGR) as a disease model for several reasons. First, it is a prevalent disease that affects around 7% of pregnancies in developed countries (WHO, 2012), and is thus a major public health issue. Late-onset IUGR is the most prevalent form and it has clearly been demonstrated to be associated with an increased risk of neurodevelopmental disorders in offspring (Bassan et al., 2011; Eixarch et al., 2008; Figueras et al., 2009; McCowan et al., 2002). Secondly, IUGR is a chronic condition which produces brain reorganization, more than overt brain damage (Rees et al., 2011), and this requires the use of advanced analysis of non-conventional brain imaging techniques to be identified (Gratacos, 2012). Finally, the early detection of infants with a high risk of neurodevelopmental problems is a challenge to modern medicine. Diagnosis in perinatal or very early life would open a window of opportunity for the treatment of these patients, which would have a strong impact on modifying clinical practice.

Here, we extracted the individual brain networks of 63 one year old infants, 41 who suffered prenatal late-onset IUGR and 22 controls, based on GM morphological similarities. Based on the analysis of the networks obtained, we tested the hypothesis that alterations in the brain network topology produced by IUGR can be assessed by GM morphology similarity based brain networks, and that network features obtained are associated with abnormal neurodevelopment later in life. Although the differences obtained were not so evident as those demonstrated by means of brain networks derived from diffusion MRI in a similar population of IUGR infants (Batalle et al., 2012), we were able to demonstrate alterations in the organization of late-onset IUGR extracted brain network topology. In addition, we provide evidence of the association of the obtained network features with neurodevelopmental scores. The proposed methodology stands as a potential candidate to develop quantitative imaging biomarkers for the prediction of the high risk of altered neurodevelopment in subjects who suffered perinatal damage and, importantly, it could be extended to other pathologies.

Materials and methods

Subjects

This study was part of a larger prospective research program on IUGR involving fetal assessment and short- and long-term postnatal follow-up at Hospital Clinic (Barcelona, Spain). The study protocol was approved by the local Ethics Committee, and written informed consent was obtained from the parents or legal guardians of all participants. The study included a sample of 84 singleton pregnancies with 51 late-onset IUGR and 33 control fetuses. Late-onset IUGR was defined as those fetuses with an estimated fetal weight (EFW) below the 10th centile according to local reference standards confirmed at birth (Figueras et al., 2008) delivered after 34 weeks of pregnancy. Control subjects were defined as fetuses with EFW between the 10th and 90th customized centiles according to local reference (Figueras et al., 2008) confirmed at birth. Pregnancies were dated according to the first-trimester crown-rump length measurements (Robinson and Fleming, 1975). Infants with chromosomal, genetic, or structural defects and signs of intrauterine infection or neonatal early onset sepsis were excluded from this study. Neonatal data were prospectively recorded including: gestational age (GA), birth weight, cephalic perimeter, gender, and neonatal complications including late-onset sepsis, necrotizing enterocolitis and chronic lung disease (defined as oxygen need at 36 weeks postmenstrual age). Maternal education was recorded as elementary or less, high school, undergraduate degree, and graduate/post-graduate degree. Maternal smoking status during pregnancy and breastfeeding were also recorded.

MRI data acquisition

Children were scanned at 12 $\pm$ 2 months corrected age, during natural sleep without sedation (Padilla et al., 2012). The scan was performed with a TIM TRIO 3.0 T whole body MR scanner (Siemens, Germany). High resolution structural T1-weighted images were obtained by a Magnetization Prepared Rapid Acquisition Gradient Echo (MPRAGE) sequence with the following parameters: 0.9-mm slice thickness with no interslice gap, 192 sagittal slices, in-plane acquisition matrix of 256×256, FoV $= 220 \times 220$ mm^2, TR $= 2050$ ms, TE $= 2.41$ ms and inversion time (TI) $= 1050$ ms. T1 acquisition time was 5 min 52 s. In addition, structural T2-weighted images were also acquired in order to exclude white matter (WM) abnormalities. All acquired images were visually inspected for apparent or aberrant artifacts, and subjects excluded accordingly. Prior to any further analyses, all the anatomical acquisitions were manually realigned to a common orientation aligning anterior and posterior commissure in the sagittal plane (pitch), and using the medial longitudinal fissure to align coronal (roll) and axial plane (yaw).

Brain segmentation and parcellation

The methodology performed to segment and parcel the brain in a similar population was previously described in Batalle et al. (2012). Briefly, the acquired images of each subject were first skull-stripped (Smith, 2002). All the resulting brain volumes were segmented into WM, GM and cerebrospinal fluid (CSF) using the unified segmentation model (Ashburner and Friston, 2005) available with the SPM software (SPM8 release, www.fil.ion.ucl.ac.uk/spm/). The default tissue probability maps of SPM were replaced by a specific one year old infant template (Shi et al., 2011). Each subject brain was regionally parceled in the native space with an atlas based on the Anatomical Automatic Labeling (AAL) atlas of 116 regions (Tzourio-Mazoyer et al., 2002), recently adapted to a one year old population (Shi et al., 2011). In order to automatically parcel each subject's brain using this atlas, we used a customized software implementing a consistent version (Tristan-Vega and Arribas, 2007) of a block matching algorithm (Warfield et al., 2002), obtaining an elastic transformation matching the template with each

Table 1
Regions of interest used as nodes in structural brain networks, corresponding to the regions defined in AAL atlas.

Anatomical regions	Label	Anatomical regions	Label
Precentral gyrus	PRE	Lingual gyrus	LING
Superior frontal gyrus, dorsolateral	F1	Superior occipital gyrus	O1
Superior frontal gyrus, orbital	F1O	Middle occipital gyrus	O2
Middle frontal gyrus	F2	Inferior occipital gyrus	O3
Middle frontal gyrus, orbital part	F2O	Fusiform gyrus	FUSI
Inferior frontal gyrus, opercular part	F3OP	Postcentral gyrus	POST
Inferior frontal gyrus, triangular part	F3T	Superior parietal gyrus	P1
Inferior frontal gyrus, orbital part	F3O	Inferior parietal, but supramarginal and angular gyri	P2
Rolandic operculum	RO	Supramarginal gyrus	SMG
Supplementary motor area	SMA	Angular gyrus	AG
Olfactory cortex	OC	Precuneus	PQ
Superior frontal gyrus, medial	F1M	Paracentral lobule	PCL
Superior frontal gyrus, medial orbital	F1MO	Caudate nucleus	CAU
Gyrus rectus	GR	Lenticular nucleus, putamen	PUT
Insula	IN	Lenticular nucleus, pallidum	PAL
Anterior cingulate and paracingulate gyri	ACIN	Thalamus	THA
Median cingulate and paracingulate gyri	MCIN	Heschl gyrus	HES
Posterior cingulate gyrus	PCIN	Superior temporal gyrus	T1
Hippocampus	HIP	Temporal pole: superior temporal gyrus	T1P
Parahippocampal gyrus	PHIP	Middle temporal gyrus	T2
Amygdala	AMYG	Temporal pole: middle temporal gyrus	T2P
Calcarine fissure and surrounding cortex	V1	Inferior temporal gyrus	T3
Cuneus	Q	Cerebellum	CER
		Vermis	VER

subject's anatomical T1 volume. The labels of the AAL atlas were propagated to each structural MRI acquisition of our subjects using this elastic transformation, with discrete labeling values preserved by nearest neighbor interpolation. The original atlas is composed of 90 cortical and sub-cortical regions and 26 cerebellar regions. In order to simplify the analysis, we merged the cerebellar regions into right cerebellum, left cerebellum and vermis, resulting in a total of 93 regions per subject brain (Table 1).

Extraction of brain networks

In the present study we followed the methodology proposed by Tijms et al. (2012) to extract individual structural morphology brain networks from MRI and extended it in order to normalize these networks to a common comparable framework based on the regional AAL parcellation previously performed. Fig. 1 shows a schematic overview of the methodology. Firstly, the GM segmentation of each individual was divided in cubes of $5 \times 5 \times 5$ voxels. We only considered non-empty cubes, which we defined as those with at least 50% of the voxels in the cube containing GM. The chosen size of $5 \times 5 \times 5$ corresponds to $4.3 \times 4.3 \times 4.5$ mm^3, slightly inferior to the cube size selected by Tijms et al. ($6 \times 6 \times 6$ mm^3), but that in our opinion maintains a good compromise between capturing the cortical folding of the brain (taking into account the smaller brain size of our subjects), and producing a reasonably detailed network, with a computationally manageable amount of cubes for each individual. Specifically, we obtained an average of 7426.6 (standard deviation = 652.2) cubes per subject. Each cube represents a node v of what we called the "weighted raw network" (WRN) of each individual, that is the network which every edge represents the similarity between each pair of cubes. In order to construct the edges of the raw network, we quantified the structural morphology similarity of two nodes v_i and v_j based on its correlation coefficient r_{ij} (Tijms et al., 2012):

$$r_{ij} = \frac{\sum_{k=1}^{n}(v_{ik}-\overline{v_i})\left(v_{jk}-\overline{v_j}\right)}{\sqrt{\sum_{k=1}^{n}(v_{ik}-\overline{v_i})^2}\sqrt{\sum_{k=1}^{n}\left(v_{jk}-\overline{v_j}\right)^2}} \quad (1)$$

Where v_{ik} is the kth element of the n voxels of the cube v_i and $\overline{v_i}$ is the mean value of all the voxels belonging to the cube v_i. The correlation coefficient was calculated for rotations of 90° and reflections over all axes of each cube, and the maximum correlation value and its corresponding p-value was taken. Finally, the "binary raw network" (BRN) of each individual was obtained by a binarization of the WRN considering only the significant correlations after a Bonferroni correction. Thus far, we have obtained a BRN of each individual similarly to Tijms et al. (2012). However, due to the methodological design, each subject would have a BRN with a different size (number of nodes), which is critical in order to compare the network features of clinical groups, given that most of the typical network features vary depending on changes in network size (van Wijk et al., 2010). For this reason, we normalized BRN based on the previously obtained AAL parcellation of each subject's brain, resulting in all subjects having the same number of nodes (93), corresponding to the different ROIs of the AAL atlas. To perform the normalization, a ROI of the AAL was assigned to each BRN node (cube), defined as the ROI to which most of the voxels of such cube belong to (mode). Each ROI constituted a node v^{norm} of what we defined as the "weighted normalized network" (WNN). Each pair of WNN nodes v_i^{norm} and v_j^{norm} were considered to be connected with a weight w_{ij} corresponding to the ratio of actual significant correlations by the total possible connections between all the BRN nodes belonging to the ROIs i and j:

$$w_{ij} = \frac{\sum_{k=1}^{N_i}\sum_{l=1}^{N_j} p_{kl}^{sig}}{N_i N_j} \quad (2)$$

Where p_{kl}^{sig} is 1 when $p_{kl}^{bonf} < 0.05$ and 0 otherwise, p_{kl}^{bonf} is the Bonferroni corrected significance of the correlation between cubes v_k and v_l, and N_i and N_j is the number of BRN nodes (cubes) belonging to ROI i and j respectively. Note that the weight obtained is bounded between 0 and 1 ($w_{ij} \in [0,1]$). Self-connections were excluded (i.e.: $w_{ii} = 0 \; \forall \; i$).

It is worth noting that in this study, we use the term "connections" to refer to brain network edges indicating statistically similar gray matter morphology of two cubes, in a similar way

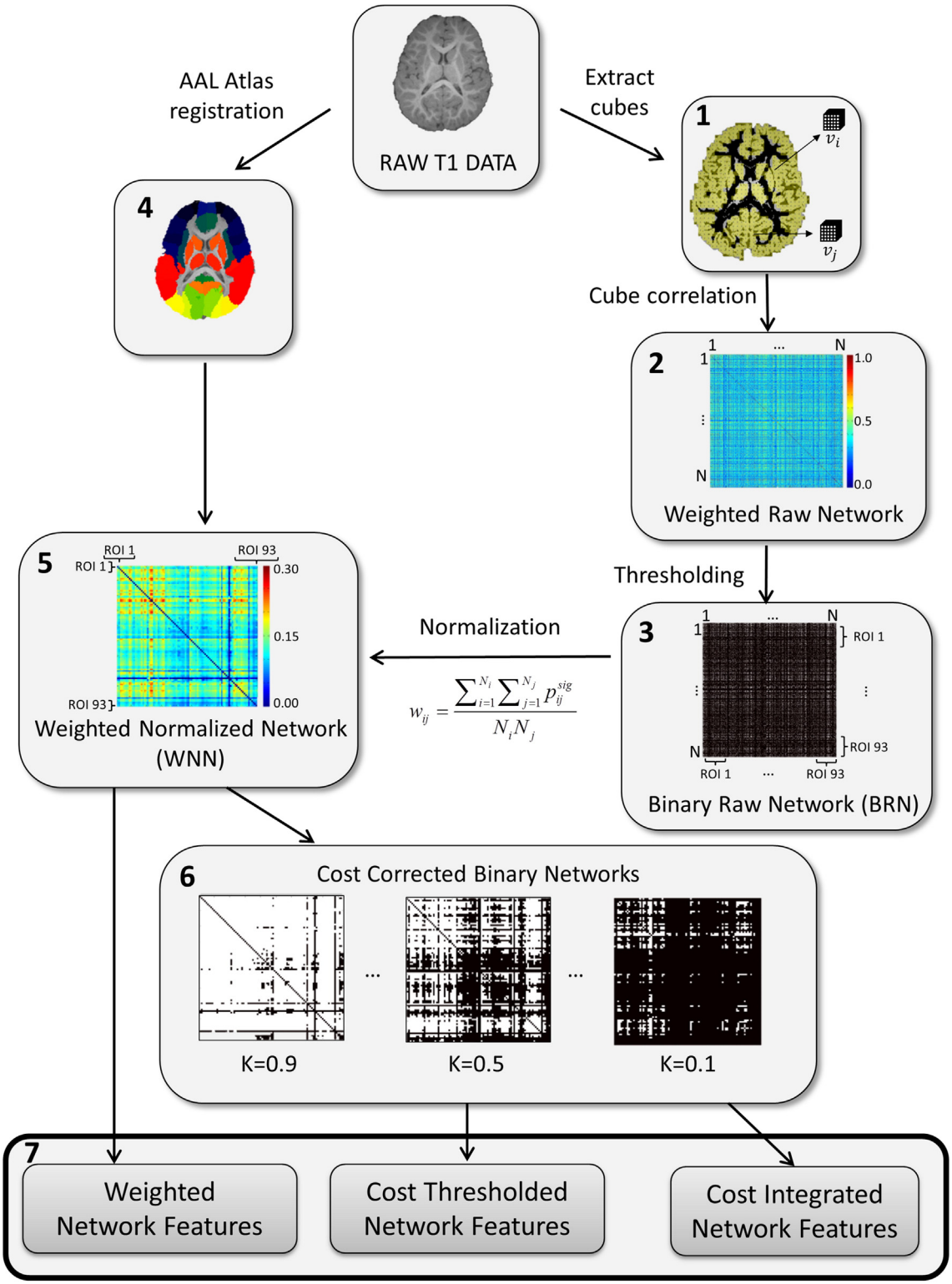

Fig. 1. General methodological scheme. (1) The GM segmentation of each individual was divided into cubes of 5 ×5 × 5 voxels. (2) The morphological similarity of each pair of cubes was calculated by its correlation coefficient obtaining the weighted raw network (WRN) of each subject. (3) Each WRN was thresholded considering only significant correlations after a Bonferroni correction, obtaining the binary raw network (BRN) of each subject. (4) Each subject brain volume was parceled in 93 ROIs corresponding to AAL atlas. (5) Information of BRN and anatomical parcellation of each subject was integrated in the weighted normalized network (WNN). (6) Cost correction of WNN was applied in order to obtain a set of binary networks corresponding to the whole range of network costs from 1 to 0 at steps of 0.01. (7) Weighted network features were obtained directly from WNN and cost-thresholded and cost-integrated network features were obtained from previously computed cost corrected binary networks.

than used previously by Tijms et al. (2012), but it must not be confused with anatomical connections. In the same line, "individual structural morphology brain networks" is used to refer to the brain networks obtained with this methodology, as the networks obtained are strongly associated with the similarity of local thickness and folding structure of different parts of the cortex, but

its relation with underlying brain connectivity still must be elucidated.

Network analysis

Graph theory measures

We mostly used definitions and nomenclature compiled by Rubinov and Sporns (2009). Briefly, N was defined as the set of all nodes in the network, and n as the number of nodes; (i,j) was the link between nodes i and j; and a_{ij} the connection status between node i and j: $a_{ij} = 1$ when link (i,j) exists and zero otherwise. w_{ij} is defined as the weight of the link (i,j) in weighted networks, normalized between 0 and 1, where a higher weight indicated a higher "connectivity" between nodes i and j. Degree of a node i was calculated as $k_i = \sum_{j \in N} a_{ij}$. Directly related to the average degree of a network, we defined the network cost K as the ratio of actual links present on a network divided by all the possible links:

$$K = \frac{1}{n(n-1)} \sum_{i,j \in N} a_{ij} \tag{3}$$

Weighted degree of a node is often called nodal strength and is calculated as the sum of all neighboring link weights of a given node: $k_i^w = \sum_{j \in N} w_{ij}$. Its average value along all nodes for a given network is a measure directly related to the energy of a network and was called average network strength.

Shortest path length between nodes i and j was defined for binary networks as $d_{ij} = \sum a_{uv} \in g_{i \leftrightarrow j}$, where $g_{i \leftrightarrow j}$ is the shortest path (geodesic) between i and j. Shortest path length was generalized for weighted networks as $d_{ij}^w = \sum a_{uv} \in g_{i \leftrightarrow j}^w f(w_{uv})$, where f is a map from weight to length (in our case an inverse map) and $g_{i \leftrightarrow j}^w$ is the shortest weighted path between i and j.

Global efficiency was defined as the average inverse shortest path length (Latora and Marchiori, 2001):

$$E_{glob} = \frac{1}{n} \sum_{i \in N} \frac{\sum_{j \in N, j \neq i} d_{ij}^{-1}}{n-1} \tag{4}$$

Generalized to weighted networks as:

$$E_{glob} = \frac{1}{n} \sum_{i \in N} \frac{\sum_{j \in N, j \neq i} \left(d_{ij}^W\right)^{-1}}{n-1} \tag{5}$$

Nodal efficiency of a node i was defined as the inverse of the harmonic mean of the minimum path length between that index node and all other nodes in the network (Achard and Bullmore, 2007):

$$E_{nodal}(i) = \frac{1}{k_i(k_i-1)} \sum_{j,h \in N, [j,h] \neq i} a_{ij} a_{ih} \left[d_{jh}(N_i)\right]^{-1} \tag{6}$$

Where $d_{jh}(N_i)$ is the length of the shortest path between j and h, which contains only neighbors of i.

Local efficiency was defined as the average of nodal efficiency of each node:

$$E_{loc} = \frac{1}{n} \sum_{i \in N} E_{nodal}(i) = \frac{1}{n} \sum_{i \in N} \frac{1}{k_i(k_i-1)} \sum_{j,h \in N, [j,h] \neq i} a_{ij} a_{ih} \left[d_{jh}(N_i)\right]^{-1} \tag{7}$$

Generalized to weighted networks as (Rubinov and Sporns, 2009):

$$E_{loc}^w = \frac{1}{n} \sum_{i \in N} \frac{1}{k_i(k_i-1)} \sum_{j,h \in N, [j,h] \neq i} \left(w_{ij} w_{ih} \left[d_{jh}^w(N_i)\right]^{-1}\right)^{\frac{1}{3}} \tag{8}$$

Levels of analysis: weighted, cost level thresholding and cost integration measures

We analyzed the obtained networks with three different approaches. The first and straightforward approach is to directly apply weighted versions of graph theory measures to the obtained WNN. However, some authors suggest that some of these measures could be closely associated with the average network strength and degree (Ginestet et al., 2011; van Wijk et al., 2010). Therefore, in order to assess the topology of weighted networks independently of its strength and cost, a set of cost level thresholds was applied to each individual weighted network, obtaining a binary network at each cost level (Ginestet et al., 2011). This second approach allows comparing networks with the same number of binary connections, and therefore, comparing network features independently of their cost. This approach, however, increases the number of comparisons and the complexity of the results interpretation, as the clinical groups must be compared at each cost threshold level. Finally, in order to disentangle connectivity strength from topology in a single value for each graph theory feature, Ginestet et al. (2011) demonstrated the usefulness of integrating each network feature over the entire cost regime. The cost-integrated version of a topological metric $T(\cdot)$ is defined as (Ginestet et al., 2011):

$$T_{CI}(G) = \frac{1}{N_I} \sum_{t=1}^{N_I} T(\gamma(G, k_t)) \tag{9}$$

Where G is a given weighted graph, $\gamma(G,k)$ is the graph G binarized at cost k_t and N_I is the cardinal of network costs assessed.

To summarize, for each individual network we computed three features: network average strength, global efficiency and local efficiency. Each of these network features was calculated in its weighted form, binarized at a cost threshold from 0 to 1 at steps of 0.01 and cost-integrated along the entire cost regime. In addition, regional analysis of network features was also performed, assessing nodal strength and nodal weighted efficiency for each network node.

Neurodevelopmental assessment

Neurodevelopmental outcome of each subject was assessed at 21 ± 2 months of corrected age with the Bayley Scale for Infant and Toddler Development, Third edition (BSID-III), which evaluates five distinct scales: cognitive, language, motor, socio-emotional behavior and adaptive behavior. The scales have scores with a mean of 100 and S.D. of 15. Abnormal Bayley was defined as a score below 85 in any of the five different scales (Anderson et al., 2010). Bayley's severity score was defined as the sum of scales below 85, being in a range from 0 to 5. All developmental examinations were performed by a single trained psychologist examiner with previous experience with the BSID-III. The examiner was not informed about the infant's medical history.

Statistical analysis

Group differences

Differences in total GM volume and regional AAL regions were assessed by means of general linear model with gender, maternal education, smoking during pregnancy and breastfeeding as cofactors and GA as covariate. In order to assess the differences in the topology of the extracted networks in the IUGR group when compared with controls, statistical comparisons among groups were also performed by means of general linear model with the same cofactors and covariates as previously, but including total GM volume as covariate to exclude GM size as a factor explaining the differences found. This was performed at the three levels of network analysis: weighted, cost level thresholding and cost integration measures. Multiple comparisons correction was

applied for regional analysis, including the results after a False Discovery Rate (FDR) over the 93 regions assessed (Benjamini et al., 2006).

Association with neurodevelopment

In order to assess the association of graph theory features obtained from the networks extracted for one-year-old children with late-onset IUGR with the neurodevelopmental scores obtained by the same children at two years of age, we followed two different approaches.

In the first approach, we computed a general linear model with normal/abnormal Bayley as independent variables and the previously analyzed network features (weighted and cost-integrated average strength, global and local efficiency) as dependent variables; gender, education, smoking during pregnancy and breastfeeding as cofactors; and GA and weight percentile as covariables. This way we assessed if there was a significant difference in the network features between IUGR children with abnormal values in their neurodevelopmental tests when compared with those with normal values, and therefore, if graph theory features obtained with the proposed methodology at one year of age have the potential to discriminate those children that will have an abnormal neurodevelopment one year after an MRI scan.

In the second approach, we assessed the association of the obtained network features with the severity of the abnormal neurodevelopment, and to which extent they added information to the clinical data. In order to do so, we first did an ordinal regression of the Bayley's severity score with the clinical data and then added graph theory features to the model in order to assess to what extent there is a better association. Note that association with neurodevelopment was performed only in the IUGR group, and weight percentile was added to clinical data as it may be relevant when group is not taken into account.

Results

Sample

Structural MRI evaluation revealed the presence of anomalies in 6 IUGR (two increased cisterna magna, one ventricular dilatation, one WM lesions and one thin corpus callosum) and in 2 controls (two increased cisterna magna) that were excluded from the final analysis. In addition, 9 controls and 4 IUGR did not pass quality criteria concerning motion artifacts that prevented performing further analysis. Thus, the final sample included 41 IUGR infants and 22 control infants.

As expected, anthropometric measurements at birth were significantly lower in the IUGR group: birth weight centile: 53.5 (32.9) vs. 2.3(2.7) $p < 0.001$, and cephalic perimeter at birth centile: 38.9 (25.1) vs. 12.7 (16.0), $p < 0.001$. GA at delivery was significantly lower in the IUGR group: 39.5 (1.5) vs. 38.1(1.6), $p = 0.003$. No significant differences were found in gender distribution: male/female 10/12 vs. 26/15, $p = 0.170$. No neonatal complications occurred among groups. No differences were observed in demographic characteristics including maternal age, maternal education and breastfeeding. However, maternal smoking status during pregnancy was increased in the IUGR group: 4.5% vs. 31.7%, $p = 0.023$. For the BSID-III neurodevelopmental test, IUGR infants showed lower scores than the control group in all scales without reaching statistical significance: Cognitive: 102.8 (15.5) vs. 99.1 (16.5), $p = 0.533$; Language: 98.8 (19.0) vs. 90.1 (17.1),$p = 0.798$; Motor: 107.1(15.8) vs. 96.5 (15.1), $p = 0.307$; Socio-emotional: 118.0 (28.6) vs. 106.6 (26.6), $p = 0.264$; Adaptive behavior: 91.4 (15.8) vs. 86.4 (16.8), $p = 0.412$. The proportion of abnormal BSID-III scores in late-onset IUGR was 60% and the distribution of Bayley's severity scores based on the number of scales affected was: one scale 42.9%, two scales 38.1%, three scales 9.5%, four scales 0%, and five scales 9.5%.

Concerning MRI acquisition, general lineal model showed reduced GM volume in the IUGR group ($p = 0.006$). Regional volume analysis also revealed differences in individual regions (Supplementary Material), but none of them were significant after FDR correction.

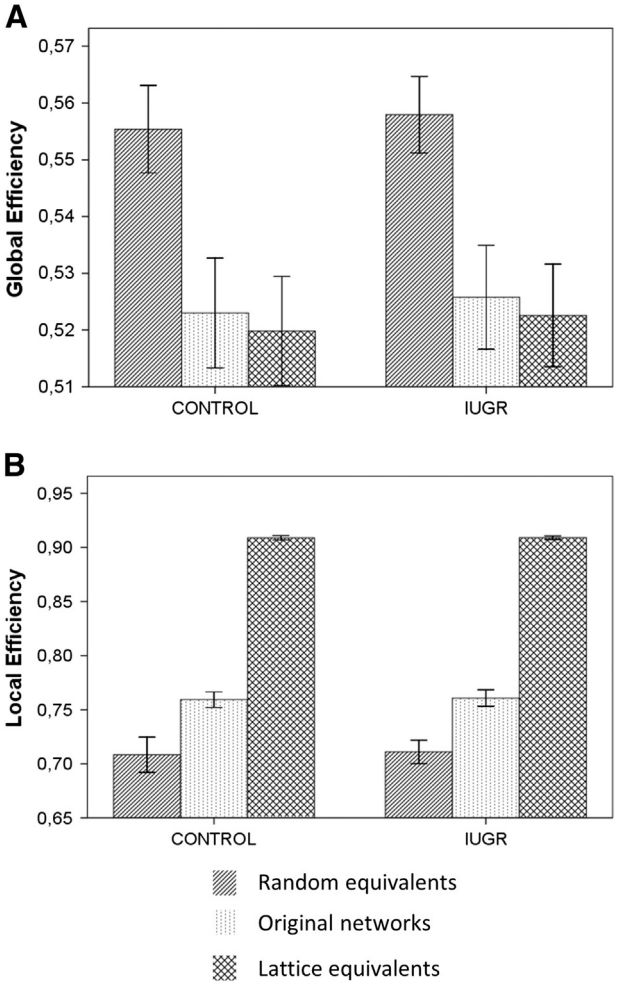

Fig. 2. Small-worldness. (A) Global and (B) local efficiency of the binary raw networks obtained compared with the values obtained for their random and lattice network equivalents.

Small-worldness

We calculated the BRN random and lattice equivalents of each subject that preserve degree distribution and compared their global and local efficiency with the original network. The original networks have an intermediate value of global and local efficiency when compared with their random and lattice equivalent, both at individual and group level, a typical characteristic of small-world networks (Fig. 2). However, the values of global and local efficiency of the original WNN and its random and lattice equivalents were virtually identical. Thus, the evaluation of small-worldness in WNN rendered unconclusive results.

Analysis of network features in IUGR

Compared with controls, analysis of global weighted features of WNN in IUGR showed no significant differences in network average strength ($p = 0.296$ $F = 1.130$), global efficiency ($p = 0.198$ $F = 1.727$) and local efficiency ($p = 0.247$ $F = 1.391$).

In order to analyze WNN independently of its network cost, thresholding and binarizing of WNN along a range of cost-levels from 0 to 1 at 0.01 steps was performed. Binary network features were analyzed at each cost level, obtaining no significant differences for average strength, some differences on local efficiency, but several in global efficiency, as shown in Fig. 3.

Integration of binary network features along the whole range of cost-levels allowed us to obtain a single representative value of each

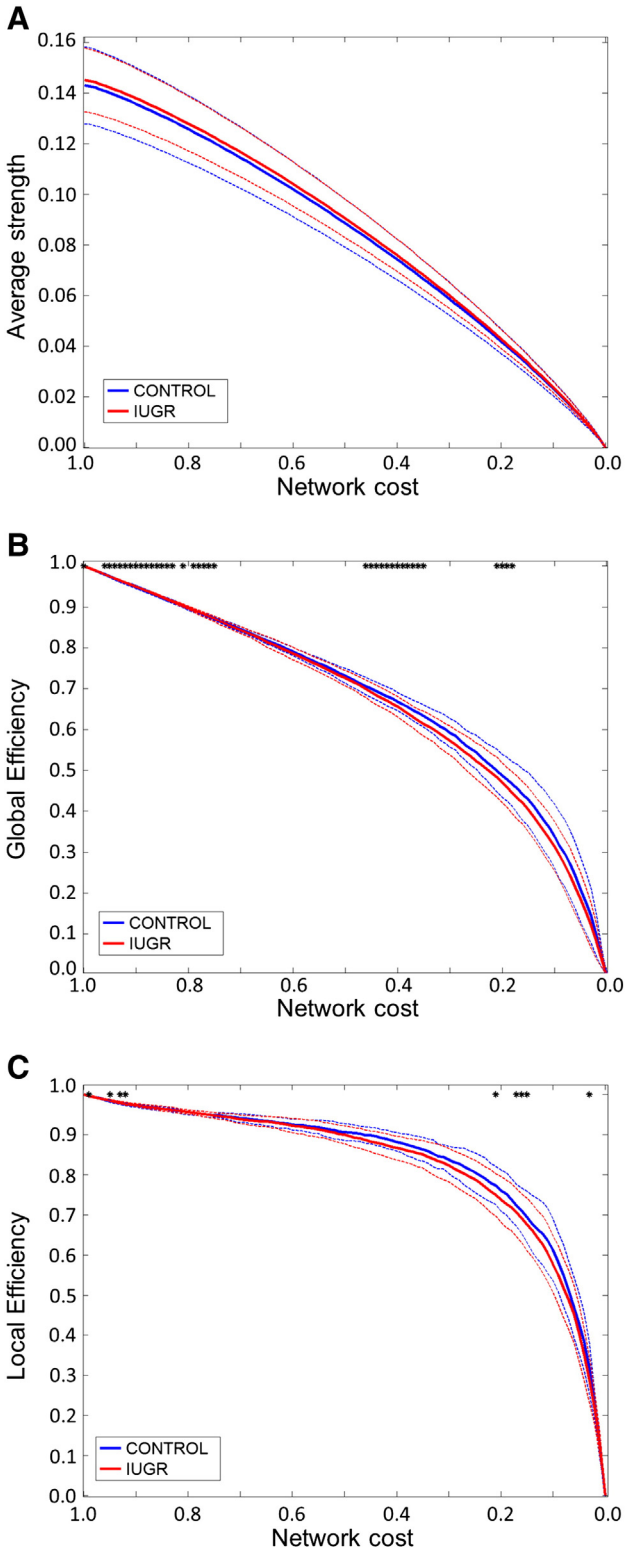

Fig. 3. Cost-thresholded network features. Control and IUGR cost-thresholded network features estimated from binarized weighted normalized networks at steps of 0.01 of network cost. (A) Average strength, (B) global efficiency and (C) local efficiency. Solid line corresponds to the mean across individuals and dashed lines to mean ± standard deviation. *p < 0.05.

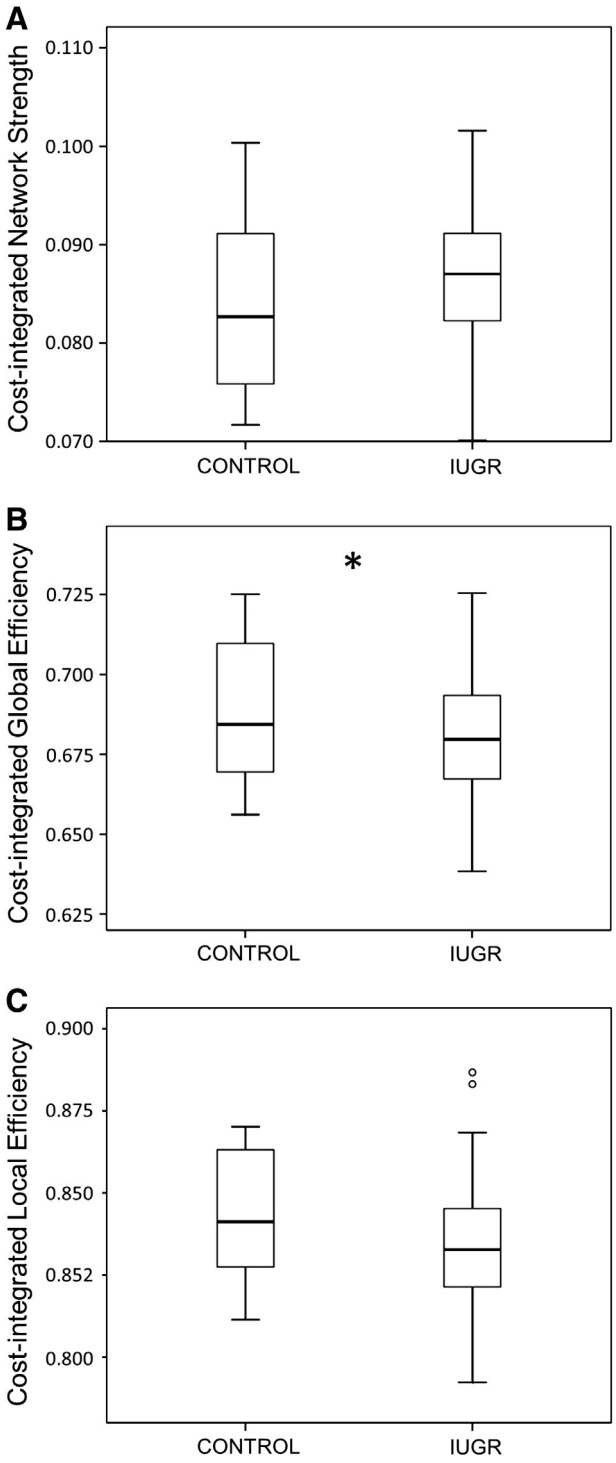

Fig. 4. Cost-integrated network features. Box plot of control and IUGR cost-integrated features. (A) Average strength, (B) global efficiency and (C) local efficiency. *p < 0.05.

binary feature that is independent of the network cost (Fig. 4). No significant difference was found on cost-integrated average strength ($p = 0.348$ $F = 0.906$) when compared with control group. Similarly, local efficiency was also not significantly different between controls and cases, although a tendency could be observed ($p = 0.076$ $F = 5.176$). However, global efficiency was significantly reduced in the IUGR group ($p = 0.030$ $F = 5.176$).

Regional network analysis of IUGR weighted networks showed differences in different regions when compared with controls. Specifically, we found alterations in left superior frontal gyrus orbital part (F1O), right parahippocampal gyrus (PHIP), left lingual gyrus (LING), left supramarginal gyrus (SMG), left angular gyrus (AG) and vermis (VER) weighted nodal efficiency and/or nodal strength (Fig. 5). However, none of them were significant after a false discovery rate correction.

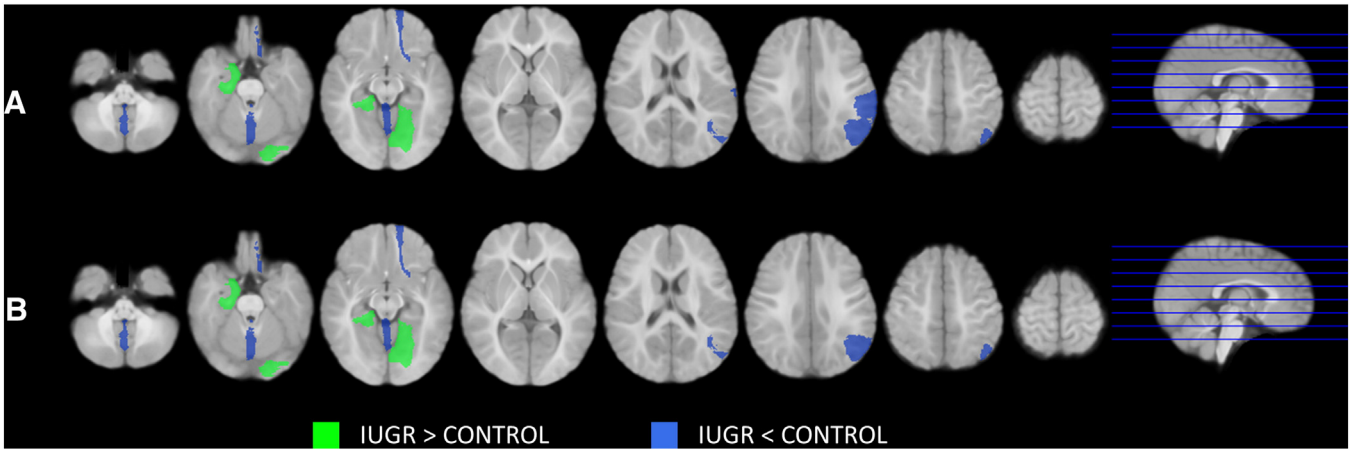

Fig. 5. Regional network features. (A) Nodal strength and (B) nodal efficiency features altered in IUGR group. Regional features highlighted in green are increased in IUGR group and those in blue are decreased.

Association with abnormal neurodevelopment in IUGR

A multivariate general linear model with the previously analyzed, weighted- and cost-integrated network features as dependent variables, and clinical features as covariables, showed no significant differences for any of the network features independently, but did show a multivariate statistically significant difference between normal and abnormal Bayley (Wilks' Lambda of 0.125, $p = 0.036$, $F = 5.815$). This demonstrated a discernibly different configuration of network features between IUGR cases with normal and abnormal Bayley.

In addition, an ordinal regression of Bayley's severity score with clinical data (GA, weight centile, gender, maternal education, smoking during pregnancy and breastfeeding) and the same ordinal regression with the addition of network features (weighted and cost integrated global efficiency, local efficiency and average strength) was also performed, demonstrating that the ordinal regression with only clinical data does not significantly fit Bayley's severity score ($p = 0.154$ $Chi^2 = 11.947$ Nagelkerke $R^2 = 0.309$, $df = 8$), but the addition of network features significantly changed the model ($p = 0.023$ $Chi^2 = 14.703$, $df = 6$), such that the resulting model was statistically significant ($p = 0.029$ $Chi^2 = 25.650$ Nagelkerke $R^2 = 0.555$, $df = 14$), demonstrating significant association of network features as a group and significantly adding information to the clinical data.

Discussion

This study, to the best of our knowledge, describes for the first time the use of individual similarity-based brain networks extracted from GM using standard T1-weighted MRI acquisitions in a pediatric population. To do so, we proposed a methodology in order to normalize the large-scale networks obtained to a common framework defined by an anatomical atlas, and applied it to a pediatric population of one-year-old infants who had suffered late-onset IUGR. Based on the networks extracted using this methodology, we demonstrated that late-onset IUGR children had an altered network topology compared with controls, and that the network features obtained are associated with the neurodevelopmental outcomes of the IUGR group at two years of age.

Individual networks obtained from GM morphology similarities

Obtaining brain networks from standard T1 anatomical acquisitions has a series of advantages compared with those reconstructed from other modalities such as diffusion or functional MRI, mainly reduced acquisition times, which is crucial in the study of several pathologies, especially in the pediatric population. There is a broad range of studies in the literature that obtained brain networks from T1 anatomical acquisitions by means of correlation of GM features, such as volume or cortical thickness, across groups of individuals. In this way, it has been possible to obtain a single brain network corresponding to a group of subjects. This line of research has been relevant to study alterations in brain organization produced by certain pathologies (Bassett et al., 2008; Bernhardt et al., 2011; He et al., 2008; Liu et al., 2008), and to improve understanding of the organization of the brain during neurodevelopment (Fan et al., 2011). However, this kind of approach is not useful to develop individual biomarkers predictive of neurological outcome as it generates only one brain network per group of individuals. Hence, developing methodologies that are able to extract individual networks from standard T1 MRI acquisitions is very relevant for clinical practice. The proposed methodology to extract individual networks benefits from the analytical power of graph theory and network models to describe GM similarities in the brain. However, it is very important to note that the extent to which the networks obtained resemble anatomical brain connectivity is an issue that requires deeper study. This issue aside, some studies have proposed that covariation of cortical morphology may be related to cortical connectivity (Andrews et al., 1997; Gong et al., 2011; Kennedy et al., 1998). Furthermore, in large-scale similarity-based networks, Tijms et al. (2012) found some similarities between the values of clustering and small world coefficients with resting-state functional MRI and morphological inter-subject correlation networks. Taking into account that some of the subjects analyzed in the present paper have available diffusion MRI included in a previous study (Batalle et al., 2012), we have performed correlations of the global graph theory features obtained with the ones generated from diffusion MRI in 10 control subjects (Supplementary Material). In this reduced sample we found correlations between weighted global and local efficiency of GM morphology similarity based brain networks with binary and weighted efficiencies obtained from diffusion MRI based brain networks. Yet even if some of the correlations found may indicate an association of the networks found in this study with underlying structural brain connectivity, it is still not clear to which extent the networks obtained in the present study resemble actual neuronal connections.

Disrupted network features in IUGR

Network features obtained with the proposed methodology in late-onset IUGR showed several differences when compared with controls when the weighted networks were binarized for the whole range of network cost. These differences are confirmed by the integration of the values along the entire cost regime, which has been proven to be a

robust measure of disentangling network topology from network cost in a single value (Ginestet et al., 2011). However, when applying the weighted versions of the features assessed directly on the weighted network, no differences were found. This can be explained as weighted measures and thresholded binary cost measures along the whole rank of network cost are assessing different aspects of network topology and are therefore complementary measures. Nodal network features revealed a pattern of mild alterations distributed along the whole brain, including regions of the frontal, occipital and parietal cortex, however, the significance of these findings is hampered after correction for multiple comparisons. Interestingly, a previous study of MRI based connectomics on IUGR babies (Batalle et al., 2012) also found decreased global and local efficiency in IUGR group, and some of the regional alterations found in the present study, as is the case of lingual gyrus, supramarginal gyrus, angular gyrus and vermis. We acknowledge that the meaning of these findings is unclear. We speculate that these differences could reflect a subtle pattern of alterations in cortical morphology produced by brain reorganization. This notion is in line with previous studies demonstrating structural differences in early and late-onset IUGR. Studies in preterm neonates have reported a decreased volume in cortical GM (Tolsa et al., 2004) and hippocampus (Lodygensky et al., 2008), and major delays in cortical development with discordant patterns of gyrification and a pronounced reduction in cortical expansion (Dubois et al., 2008). Persistence of structural changes at one year of age in IUGR babies has been reported, which demonstrate reduced volumes of GM in the temporal, parietal, frontal and insular regions (Padilla et al., 2011) and decreases in the fractal dimension of both gray and white matter, which correlate with specific neurodevelopmental difficulties in a similar population (Esteban et al., 2010). Note that the importance of the relationship between the network features obtained by individual GM similarity-based networks and fractal dimension has been previously suggested as there is a resemblance in both methodologies (Tijms et al., 2012). Recently published data has also demonstrated a reduced global cortical surface and volume as well as regional changes in cortical thickness, especially in the frontal region, in children after late-onset IUGR (De Bie et al., 2011) such that these regional changes are also present in the adolescent population (Martinussen et al., 2005).

Association of network features obtained with abnormal Bayley's scales in IUGR

Concerning the neurodevelopmental tests, late-onset IUGR showed lower results in all Bayley's scales, although reduced sample size prevented us from finding significant differences. Nevertheless, an association between IUGR and long-term neurodevelopmental and cognitive dysfunctions has been previously demonstrated (Bassan et al., 2011; Feldman and Eidelman, 2006; Geva et al., 2006a,b; Leitner et al., 2007; McCarton et al., 1996; Scherjon et al., 1993) as was the case with studies focusing on late-onset cases (Bassan et al., 2011; Eixarch et al., 2008; Figueras et al., 2009; McCowan et al., 2002). Our results demonstrated that network features of brain networks extracted from GM standard T1-weighted acquisitions at one year of age are related with neurodevelopment later in life. Association between network features in the IUGR population has previously been reported using diffusion MRI based brain networks (Batalle et al., 2012). In the present study, the combination of clinical data with global features was associated with the number of abnormal Bayley's scales, giving additional information about the severity of the neurodevelopmental delay. In our opinion, it is highly relevant that the network features extracted with the present methodology are related with neurodevelopmental outcome in IUGR children, suggesting the potential of this methodology to generate biomarkers able to detect altered neurodevelopment. This is especially relevant to clinical practice as the early detection of abnormal neurodevelopment would open a window of opportunity to apply interventional strategies.

Methodological considerations

Some methodological considerations must also be discussed. First of all, it is worth noting that brain parcellation and tissue segmentation in GM and WM in the infant brain is a critical issue due to the isointense developmental pattern which results from poor differentiation of tissues (Paus et al., 2001). However, the use of high quality T1 weighted 3-T MRI minimizes this effect. In addition, it is worth noting that to improve the reliability of the results obtained we used appropriated brain tissue probability maps of one-year-old infants for tissue segmentation and a pediatric atlas for brain parcellation (Shi et al., 2011). Each scan was reviewed to exclude those cases with apparent movement artifacts. In addition, brain tissue segmentation was individually analyzed to determine if the results of the tissue segmentation were accurate. The acquisition protocol during natural sleep (Padilla et al., 2012) allowed us to obtain good quality imaging without the use of sedation and, consequently, we obtained a very high ratio of successful acquisitions, taking into account the difficulty of acquiring MRI in such a young pediatric population. Due to the characteristics of the methodological approach proposed, it is reasonable to think that different brain orientation could have some effects on the obtained brain networks. To address this effect all the subjects were manually realigned previously to any further analyses, minimizing any possible influence of the patient orientation in the obtained networks. In addition we have assessed the effect on the network stability of minor head rotations ($\pm 10°$ at 2 degree steps in each axis) in the networks extracted (Supplementary Material), showing that the intra-subject variability provoked by head rotations is lower than inter-subject variability, hence observing the relatively high stability of the networks to this effect.

Some differences between the methodology proposed here and the methods presented by Tijms et al. (2012) should also be noted. Although Tijms et al. (2012) opted for a false discovery rate approach in order to obtain the BRN, thereby correcting the significance for the high amount of voxels analyzed, we opted for a more restrictive approach, using a Bonferroni correction, by which we obtained a relatively high amount of significant correlations while minimizing the amount of false positives. In order to correct cube correlation for rotation, we used 90 degree steps instead of 45. Note that it is possible to perform correlations of cubes rotated 45° without interpolation only if the cubes have a size of three voxels. For cubes of $5 \times 5 \times 5$ voxels, as in our case, the center of some rotated voxels would fall outside the boundaries of a voxel of the other cube, making it necessary to interpolate. It is our belief that decreasing false negatives in the extracted BRN does not justify the artifacts of partial volume effects and the interpolation needed to correct rotations by 45°. Note that the modifications performed in the methodology proposed by Tijms et al. (2012) are all very conservative: in the worst case increasing false negatives in the BRN obtained, but minimizing the number of false positives.

Strengths and limitations

One of the main strengths of this methodology is the straightforward adaptation of the proposed method to different population groups where MRI is a challenge and where connectomics based on diffusion and/or functional MRI is extremely difficult to perform, such as the pediatric population. Anatomical reconstruction of fetal structural acquisitions is becoming increasingly used in the literature (Kim et al., 2010; Kuklisova-Murgasova et al., 2012; Studholme, 2011). Hence, although the networks obtained are not so detailed and they lack a clear anatomical interpretation compared with those obtained with other techniques, adapting and assessing the proposed methodology to the fetal population seems a good opportunity to obtain biomarkers based on network features at the prenatal age and is a feasible alternative until diffusion and functional MRI protocols during fetal life become reliable and standardized.

Some limitations of the proposed methodology should also be noted. By its design, the methodology presented does not discriminate between GM to CSF or GM to WM boundaries, thus a connection could be considered between two cubes that have similar GM pattern without taking into account if they are adjacent to WM or CSF. However, it must be stressed that, even if the area occupied by WM and/or CSF in a pair of cubes is identical, a connection will not be established if GM pattern between the two cubes is different.

Another key issue that can be considered a limitation of this study is the possible resemblance (or not) of the networks obtained with actual underlying brain circuitry. Some hints on the validity of the networks obtained have been shown in the original article presenting the theoretical base of this methodology (Tijms et al., 2012), comparing the individual networks obtained to resting state and conventional GM morphology inter-subject correlation networks. In addition, in the present study some correlations of the network features obtained with a reduced sample of 10 subjects with diffusion MRI based networks has also been shown (Supplementary Material). However, the evidence available is not enough to state that there is an actual underlying brain circuitry explaining the connections obtained with the present methodology. Further studies are necessary to compare the individual networks obtained from GM morphology similarities to those networks obtained from standard diffusion and/or functional MRI in larger samples to clarify this issue. This is an extremely important remark when interpreting the results obtained, but is not so relevant from the point of view of purely developing neurological outcome biomarkers. Being able to show differences in the network features obtained between controls and cases may not directly indicate a different topology of brain circuitry, but may instead be showing subtle differences in cortical patterns that may not be detected by other less sensitive techniques. We can only hypothesize that the differences found can be partially explained not only by differences in brain connectivity that modulate cortical morphology (Gong et al., 2011; Van Essen, 1997), but also by differences in cortical structure produced by other reasons, such as changes in the distribution and/or density of neuronal bodies as occurs in animal models of chronic hypoxia (Fagel et al., 2006). In any case, in the sense used in the present paper, networks represent the similarities between regions of the brain (nodes) giving the weight of this similarity to the links connecting them. Whether these links, or what is the same, the morphological similarity between regions of the brain, describe or not an underlying circuitry is certainly unknown. However, to our understanding, the relevance of the technique and results here presented lies on the fact that differences in a pathological group have been demonstrated with this methodology and, importantly, a correlation between the features of the extracted networks from a simple T1 acquisition with the neurodevelopmental tests performed one year later has been found. This data show the potential of the proposed methodology to find image biomarkers in a different set of pathologies, but especially in the pediatric population, independently of whether or not the networks obtained with the presented methodology correspond with true underlying brain circuitries.

Conclusions

The methodology presented here proposes a solution for the problem of having different network sizes in individual large-scale networks obtained from GM MRI as published by Tijms et al. (2012). To the best of our knowledge, the present paper is the first work exploring the use of individual networks based on GM features in a pediatric population. Specifically, we applied the methodology proposed in a pediatric population who suffered perinatal mild brain reorganization, which is one of the target groups that can benefit from this kind of analysis. In this population, we were able to objectively demonstrate statistically significant differences between controls and children who suffered late-onset IUGR, supporting the notion that these children, although suffering a mild chronic insult, present patterns of brain organization that are different from their healthy counterparts. A noteworthy feature is that the network features obtained were successfully associated with abnormal neurodevelopmental scores, adding statistically relevant information to clinical data, nowadays the standard for the evaluation of neurological outcome in IUGR. Although this methodology must be more widely assessed, it stands as a good candidate for the development of biomarkers for altered neurodevelopment in the pediatric population.

Funding

This work was supported by grants: Obra Social “la Caixa”, Barcelona, Spain; The Cerebra Foundation for the Brain-Injured Child, Carmarthen, Wales, UK; The Thrasher Research Fund, Salt Lake City, USA; The People Programme (Marie Curie Actions) of the European Union's Seventh Framework Programme FP7 under REA Grant Agreement number 217911 (u-Volumes); and Sara Borrell grants from Carlos III Institute of Health, Spain (grant number CD11/00048 to E.M.).

Acknowledgments

The authors would like to acknowledge Prof. Alberto Prats-Galino for useful discussions on the design of the methodology. The images used in this study were acquired in the Medical Imaging Core Facility of Institut d'Investigacions Biomèdiques August Pi i Sunyer (IDIBAPS), Barcelona, Spain.

Conflict of interest

The authors have no conflicts of interest to declare.

Appendix A. Supplementary data

Supplementary data to this article can be found online at http://dx.doi.org/10.1016/j.neuroimage.2013.07.045.

References

Achard, S., Bullmore, E., 2007. Efficiency and cost of economical brain functional networks. PLoS Comput. Biol. 3, e17.
Alexander-Bloch, A.F., Gogtay, N., Meunier, D., Birn, R., Clasen, L., Lalonde, F., Lenroot, R., Giedd, J., Bullmore, E.T., 2010. Disrupted modularity and local connectivity of brain functional networks in childhood-onset schizophrenia. Front. Syst. Neurosci. 4, 147.
Anderson, P.J., De Luca, C.R., Hutchinson, E., Roberts, G., Doyle, L.W., 2010. Underestimation of developmental delay by the new Bayley-III Scale. Arch. Pediatr. Adolesc. Med. 164, 352–356.
Andrews, T.J., Halpern, S.D., Purves, D., 1997. Correlated size variations in human visual cortex, lateral geniculate nucleus, and optic tract. J. Neurosci. 17, 2859–2868.
Ashburner, J., Friston, K.J., 2005. Unified segmentation. Neuroimage 26, 839–851.
Bassan, H., Stolar, O., Geva, R., Eshel, R., Fattal-Valevski, A., Leitner, Y., Waron, M., Jaffa, A., Harel, S., 2011. Intrauterine growth-restricted neonates born at term or preterm: how different? Pediatr. Neurol. 44, 122–130.
Bassett, D.S., Bullmore, E.T., 2009. Human brain networks in health and disease. Curr. Opin. Neurol. 22, 340–347.
Bassett, D.S., Bullmore, E., Verchinski, B.A., Mattay, V.S., Weinberger, D.R., Meyer-Lindenberg, A., 2008. Hierarchical organization of human cortical networks in health and schizophrenia. J. Neurosci. 28, 9239–9248.
Batalle, D., Eixarch, E., Figueras, F., Munoz-Moreno, E., Bargallo, N., Illa, M., Acosta-Rojas, R., Amat-Roldan, I., Gratacos, E., 2012. Altered small-world topology of structural brain networks in infants with intrauterine growth restriction and its association with later neurodevelopmental outcome. Neuroimage 60, 1352–1366.
Benjamini, Y., Krieger, A.M., Yekutieli, D., 2006. Adaptive linear step-up procedures that control the false discovery rate. Biometrika 93, 491–507.
Bernhardt, B.C., Chen, Z., He, Y., Evans, A.C., Bernasconi, N., 2011. Graph-theoretical analysis reveals disrupted small-world organization of cortical thickness correlation networks in temporal lobe epilepsy. Cereb. Cortex 21, 2147–2157.
De Bie, H.M., Oostrom, K.J., Boersma, M., Veltman, D.J., Barkhof, F., Delemarre-van de Waal, H.A., van den Heuvel, M.P., 2011. Global and regional differences in brain anatomy of young children born small for gestational age. PLoS One 6, e24116.
Dubois, J., Benders, M., Borradori-Tolsa, C., Cachia, A., Lazeyras, F., Ha-Vinh Leuchter, R., Sizonenko, S.V., Warfield, S.K., Mangin, J.F., Hüppi, P.S., 2008. Primary cortical folding in the human newborn: an early marker of later functional development. Brain 131, 2028–2041.
Eixarch, E., Meler, E., Iraola, A., Illa, M., Crispi, F., Hernandez-Andrade, E., Gratacos, E., Figueras, F., 2008. Neurodevelopmental outcome in 2-year-old infants who

were small-for-gestational age term fetuses with cerebral blood flow redistribution. Ultrasound Obstet. Gynecol. 32, 894–899.
Eliez, S., Reiss, A.L., 2000. MRI neuroimaging of childhood psychiatric disorders: a selective review. J. Child Psychol. Psychiatry 41, 679–694.
Esteban, F.J., Padilla, N., Sanz-Cortes, M., de Miras, J.R., Bargallo, N., Villoslada, P., Gratacos, E., 2010. Fractal-dimension analysis detects cerebral changes in preterm infants with and without intrauterine growth restriction. Neuroimage 53, 1225–1232.
Fagel, D.M., Ganat, Y., Silbereis, J., Ebbitt, T., Stewart, W., Zhang, H., Ment, L.R., Vaccarino, F.M., 2006. Cortical neurogenesis enhanced by chronic perinatal hypoxia. Exp. Neurol. 199, 77–91.
Fan, Y., Shi, F., Smith, J.K., Lin, W., Gilmore, J.H., Shen, D., 2011. Brain anatomical networks in early human brain development. Neuroimage 54, 1862–1871.
Feldman, R., Eidelman, A.I., 2006. Neonatal state organization, neuromaturation, mother-infant interaction, and cognitive development in small-for-gestational-age premature infants. Pediatrics 118, e869–e878.
Figueras, F., Meler, E., Iraola, A., Eixarch, E., Coll, O., Figueras, J., Francis, A., Gratacos, E., Gardosi, J., 2008. Customized birthweight standards for a Spanish population. Eur. J. Obstet. Gynecol. Reprod. Biol. 136, 20–24.
Figueras, F., Oros, D., Cruz-Martinez, R., Padilla, N., Hernandez-Andrade, E., Botet, F., Costas-Moragas, C., Gratacos, E., 2009. Neurobehavior in term, small-for-gestational age infants with normal placental function. Pediatrics 124, e934–e941.
Geva, R., Eshel, R., Leitner, Y., Fattal-Valevski, A., Harel, S., 2006a. Memory functions of children born with asymmetric intrauterine growth restriction. Brain Res. 1117, 186–194.
Geva, R., Eshel, R., Leitner, Y., Valevski, A.F., Harel, S., 2006b. Neuropsychological outcome of children with intrauterine growth restriction: a 9-year prospective study. Pediatrics 118, 91–100.
Ginestet, C.E., Nichols, T.E., Bullmore, E.T., Simmons, A., 2011. Brain network analysis: separating cost from topology using cost-integration. PLoS One 6, e21570.
Gong, G., He, Y., Concha, L., Lebel, C., Gross, D.W., Evans, A.C., Beaulieu, C., 2009. Mapping anatomical connectivity patterns of human cerebral cortex using in vivo diffusion tensor imaging tractography. Cereb. Cortex 19, 524–536.
Gong, G., He, Y., Chen, Z.J., Evans, A.C., 2011. Convergence and divergence of thickness correlations with diffusion connections across the human cerebral cortex. Neuroimage 59, 1239–1248.
Gratacos, E., 2012. Opportunities and challenges of biomedical imaging in fetal and neonatal brain disease. Proceedings of the 9th IEEE International Symposium on Biomedical Imaging: From Nano to Macro, pp. 493–494.
Hagmann, P., 2005. From Diffusion MRI to Brain Connectomics. Signal Processing Institute. Ecole Polytechnique Fédérale de Lausanne (EPFL), Lausanne.
Hagmann, P., Cammoun, L., Gigandet, X., Meuli, R., Honey, C.J., Wedeen, V.J., Sporns, O., 2008. Mapping the structural core of human cerebral cortex. PLoS Biol. 6, e159.
Hagmann, P., Sporns, O., Madan, N., Cammoun, L., Pienaar, R., Wedeen, V.J., Meuli, R., Thiran, J.P., Grant, P.E., 2010. White matter maturation reshapes structural connectivity in the late developing human brain. Proc. Natl. Acad. Sci. U. S. A. 107, 19067–19072.
He, Y., Chen, Z.J., Evans, A.C., 2007. Small-world anatomical networks in the human brain revealed by cortical thickness from MRI. Cereb. Cortex 17, 2407–2419.
He, Y., Chen, Z., Evans, A.C., 2008. Structural insights into aberrant topological patterns of large-scale cortical networks in Alzheimer's disease. J. Neurosci. 28, 8148–8159.
He, Y., Dagher, A., Chen, Z., Charil, A., Zijdenbos, A., Worsley, K., Evans, A., 2009. Impaired small-world efficiency in structural cortical networks in multiple sclerosis associated with white matter lesion load. Brain 132, 3366–3379.
Horsfield, M.A., Jones, D.K., 2002. Applications of diffusion-weighted and diffusion tensor MRI to white matter diseases — a review. NMR Biomed. 15, 570–577.
Iturria-Medina, Y., Sotero, R.C., Canales-Rodríguez, E.J., Alemán-Gómez, Y., Melie-García, L., 2008. Studying the human brain anatomical network via diffusion-weighted MRI and graph theory. Neuroimage 40, 1064–1076.
Kennedy, D.N., Lange, N., Makris, N., Bates, J., Meyer, J., Caviness Jr., V.S., 1998. Gyri of the human neocortex: an MRI-based analysis of volume and variance. Cereb. Cortex 8, 372–384.
Kim, K., Habas, P.A., Rousseau, F., Glenn, O.A., Barkovich, A.J., Studholme, C., 2010. Intersection based motion correction of multislice MRI for 3-D in utero fetal brain image formation. IEEE Trans. Med. Imaging 29, 146–158.
Kuklisova-Murgasova, M., Quaghebeur, G., Rutherford, M.A., Hajnal, J.V., Schnabel, J.A., 2012. Reconstruction of fetal brain MRI with intensity matching and complete outlier removal. Med. Image Anal. 16, 1550–1564.
Latora, V., Marchiori, M., 2001. Efficient behavior of small-world networks. Phys. Rev. Lett. 87, 198701.
Leitner, Y., Fattal-Valevski, A., Geva, R., Eshel, R., Toledano-Alhadef, H., Rotstein, M., Bassan, H., Radianu, B., Bitchonsky, O., Jaffa, A.J., Harel, S., 2007. Neurodevelopmental outcome of children with intrauterine growth retardation: a longitudinal, 10-year prospective study. J. Child Neurol. 22, 580–587.
Li, Y., Liu, Y., Li, J., Qin, W., Li, K., Yu, C., Jiang, T., 2009. Brain anatomical network and intelligence. PLoS Comput. Biol. 5, e1000395.
Liu, Y., Liang, M., Zhou, Y., He, Y., Hao, Y., Song, M., Yu, C., Liu, H., Liu, Z., Jiang, T., 2008. Disrupted small-world networks in schizophrenia. Brain 131, 945–961.
Lo, C.Y., Wang, P.N., Chou, K.H., Wang, J., He, Y., Lin, C.P., 2010. Diffusion tensor tractography reveals abnormal topological organization in structural cortical networks in Alzheimer's disease. J. Neurosci. 30, 16876–16885.
Lodygensky, G.A., Seghier, M.L., Warfield, S.K., Tolsa, C.B., Sizonenko, S., Lazeyras, F., Huppi, P.S., 2008. Intrauterine growth restriction affects the preterm infant's hippocampus. Pediatr. Res. 63, 438–443.
Martinussen, M., Fischl, B., Larsson, H.B., Skranes, J., Kulseng, S., Vangberg, T.R., Vik, T., Brubakk, A.M., Haraldseth, O., Dale, A.M., 2005. Cerebral cortex thickness in 15-year-old adolescents with low birth weight measured by an automated MRI-based method. Brain 128, 2588–2596.
McCarton, C.M., Wallace, I.F., Divon, M., Vaughan Jr., H.G., 1996. Cognitive and neurologic development of the premature, small for gestational age infant through age 6: comparison by birth weight and gestational age. Pediatrics 98, 1167–1178.
McCowan, L.M., Pryor, J., Harding, J.E., 2002. Perinatal predictors of neurodevelopmental outcome in small-for-gestational-age children at 18 months of age. Am. J. Obstet. Gynecol. 186, 1069–1075.
Padilla, N., Falcon, C., Sanz-Cortes, M., Figueras, F., Bargallo, N., Crispi, F., Eixarch, E., Arranz, A., Botet, F., Gratacos, E., 2011. Differential effects of intrauterine growth restriction on brain structure and development in preterm infants: a magnetic resonance imaging study. Brain Res. 1382, 98–108.
Padilla, N., Botet, F., Gratacos, E., 2012. MRI at 12 ± 2 months' corrected age without sedation. Pediatr. Radiol. 42, 385.
Paus, T., Collins, D.L., Evans, A.C., Leonard, G., Pike, B., Zijdenbos, A., 2001. Maturation of white matter in the human brain: a review of magnetic resonance studies. Brain Res. Bull. 54, 255–266.
Raj, A., Mueller, S.G., Young, K., Laxer, K.D., Weiner, M., 2010. Network-level analysis of cortical thickness of the epileptic brain. Neuroimage 52, 1302–1313.
Rees, S., Harding, R., Walker, D., 2011. The biological basis of injury and neuroprotection in the fetal and neonatal brain. Int. J. Dev. Neurosci. 29, 551–563.
Robinson, H.P., Fleming, J.E., 1975. A critical evaluation of sonar "crown-rump length" measurements. Br. J. Obstet. Gynaecol. 82, 702–710.
Rubinov, M., Sporns, O., 2009. Complex network measures of brain connectivity: uses and interpretations. Neuroimage 52, 1059–1069.
Scherjon, S.A., Smolders-DeHaas, H., Kok, J.H., Zondervan, H.A., 1993. The "brain-sparing" effect: antenatal cerebral Doppler findings in relation to neurologic outcome in very preterm infants. Am. J. Obstet. Gynecol. 169, 169–175.
Shi, F., Yap, P.T., Wu, G., Jia, H., Gilmore, J.H., Lin, W., Shen, D., 2011. Infant brain atlases from neonates to 1- and 2-year-olds. PLoS One 6, e18746.
Shu, N., Liu, Y., Li, J., Li, Y., Yu, C., Jiang, T., 2009. Altered anatomical network in early blindness revealed by diffusion tensor tractography. PLoS One 4, e7228.
Shu, N., Liu, Y., Li, K., Duan, Y., Wang, J., Yu, C., Dong, H., Ye, J., He, Y., 2011. Diffusion tensor tractography reveals disrupted topological efficiency in white matter structural networks in multiple sclerosis. Cereb. Cortex 21, 2565–2577.
Smith, S.M., 2002. Fast robust automated brain extraction. Hum. Brain Mapp. 17, 143–155.
Sporns, O., Tononi, G., Kotter, R., 2005. The human connectome: a structural description of the human brain. PLoS Comput. Biol. 1, e42.
Studholme, C., 2011. Mapping fetal brain development in utero using magnetic resonance imaging: the Big Bang of brain mapping. Annu. Rev. Biomed. Eng. 13, 345–368.
Tijms, B.M., Series, P., Willshaw, D.J., Lawrie, S.M., 2012. Similarity-based extraction of individual networks from gray matter MRI scans. Cereb. Cortex 22, 1530–1541.
Tijms, B.M., Moller, C., Vrenken, H., Wink, A.M., de Haan, W., van der Flier, W.M., Stam, C.J., Scheltens, P., Barkhof, F., 2013. Single-subject grey matter graphs in Alzheimer's disease. PLoS One 8, e58921.
Tolsa, C.B., Zimine, S., Warfield, S.K., Freschi, M., Sancho Rossignol, A., Lazeyras, F., Hanquinet, S., Pfizenmaier, M., Huppi, P.S., 2004. Early alteration of structural and functional brain development in premature infants born with intrauterine growth restriction. Pediatr. Res. 56, 132–138.
Tristan-Vega, A., Arribas, J.I., 2007. A fast B-spline pseudo-inversion algorithm for consistent image registration. Proceedings of the International Conference on Computer Analysis Images and Patterns (CAIP), Vienna, Austria, pp. 768–775.
Tymofiyeva, O., Hess, C.P., Ziv, E., Tian, N., Bonifacio, S.L., McQuillen, P.S., Ferriero, D.M., Barkovich, A.J., Xu, D., 2012. Towards the "baby connectome": mapping the structural connectivity of the newborn brain. PLoS One 7, e31029.
Tzourio-Mazoyer, N., Landeau, B., Papathanassiou, D., Crivello, F., Etard, O., Delcroix, N., Mazoyer, B., Joliot, M., 2002. Automated anatomical labeling of activations in SPM using a macroscopic anatomical parcellation of the MNI MRI single-subject brain. Neuroimage 15, 273–289.
Van Essen, D.C., 1997. A tension-based theory of morphogenesis and compact wiring in the central nervous system. Nature 385, 313–318.
van Wijk, B.C.M., Stam, C.J., Daffertshofer, A., 2010. Comparing brain networks of different size and connectivity density using graph theory. PLoS One 5, e13701.
Wang, L., Zhu, C., He, Y., Zang, Y., Cao, Q., Zhang, H., Zhong, Q., Wang, Y., 2009. Altered small-world brain functional networks in children with attention-deficit/hyperactivity disorder. Hum. Brain Mapp. 30, 638–649.
Warfield, S.K., Guimond, A., Roche, A., Bharatha, A., Tei, A., Talos, F., Rexilius, J., Ruiz-Alzola, J., Westin, C.F., Haker, S., Angenent, S., Tannenbaum, A., Jolesz, F., Kilkinis, R., 2002. Advanced nonrigid registration algorithms for image fusion. In: Mazziotta, J.C., Toga, A.W. (Eds.), Brain Mapping: The Methods. Elsevier, pp. 661–690.
Wee, C.-Y., Yap, P.-T., Li, W., Denny, K., Browndyke, J.N., Potter, G.G., Welsh-Bohmer, K.A., Wang, L., Shen, D., 2010. Enriched white matter connectivity networks for accurate identification of MCI patients. Neuroimage 54, 1812–1822.
Wen, W., Zhu, W., He, Y., Kochan, N.A., Reppermund, S., Slavin, M.J., Brodaty, H., Crawford, J., Xia, A., Sachdev, P., 2011. Discrete neuroanatomical networks are associated with specific cognitive abilities in old age. J. Neurosci. 31, 1204–1212.
WHO, 2012. World Health Statistics 2012. World Health Organization, Geneva.
Wu, T., Wang, L., Chen, Y., Zhao, C., Li, K., Chan, P., 2009. Changes of functional connectivity of the motor network in the resting state in Parkinson's disease. Neurosci. Lett. 460, 6–10.
Yap, P.T., Fan, Y., Chen, Y., Gilmore, J.H., Lin, W., Shen, D., 2011. Development trends of white matter connectivity in the first years of life. PLoS One 6, e24678.
Zhou, L., Wang, Y., Li, Y., Yap, P.T., Shen, D., 2011. Hierarchical anatomical brain networks for MCI prediction: revisiting volumetric measures. PLoS One 6, e21935.